"Green-reduced" graphene oxide induces *in vitro* an enhanced biomimetic mineralization of polycaprolactone electrospun meshes

Marrella[1,2‡], G. Tedeschi[1,3‡], P. Giannoni[2], A. Lagazzo[4], F. Sbrana[5], F. Barberis[4] , R. Quarto[2,6] , F. Puglisi[2], S. Scaglione[1]*

[1] CNR – National Research Council of Italy, IEIIT Institute, Via De Marini 6, 16149 Genoa, Italy

[2] Department of Experimental Medicine, University of Genoa, Largo L.B. Alberti 2, 16132 Genoa, Italy

[3] Department of Informatics, Bioengineering, Robotics and Systems Engineering, University of Genova, Via all' Opera Pia 13, 16145 Genoa, Italy

[4] Department of Civil, Chemical and Environmental Engineering, University of Genoa, via all'Opera Pia 15, 16145 Genoa, Italy

[5] CNR – National Research Council of Italy, IBF Institute, Via De Marini 6, 16149 Genoa, Italy

[6] Ospedale Policlinico San Martino, Genova, Italy.

Corresponding Author

* Tel. 0039 0106475206 E-mail: silvia.scaglione@ieiit.cnr.it

Abstract

A novel green method for graphene oxide (GO) reduction via ascorbic acid has been adopted to realize bio-friendly reduced graphene oxide (RGO)/polycaprolactone (PCL) nanofibers meshes, as substrates for bone tissue engineering applications. PCL fibrous mats enriched with either RGO or GO (0.25 wt%) were fabricated to recapitulate the fibrillar structure of the bone extracellular matrix (ECM) and the effects of RGO incorporation on the structural proprieties, biomechanics and bioactivity of the nano-composites meshes were evaluated. RGO/PCL fibrous meshes displayed superior mechanical properties (i.e. Young's Modulus and ultimate tensile strength) besides supporting noticeably improved cell adhesion, spreading, and proliferation of fibroblasts and osteoblast-like cell lines. Furthermore, RGO-based electrospun substrates enhanced *in vitro* calcium deposition in the ECM produced by osteoblast-like cells, which was paralleled, in human mesenchymal stem cells grown onto the same substrates, by an increased expression of the osteogenic markers mandatory for mineralization. In this respect, the capability of graphene-based materials to adsorb osteogenic factors cooperates sinergically with the rougher surface of RGO/PCL-based materials, evidenced by AFM analysis, to ignite mineralization of the neo-deposited matrix and to promote the osteogenic commitment of the cultured cell in the surrounding microenvironment.

Keywords

1. Introduction

Crucial challenges, in biomedicine, are the design and development of high-efficiency tissue-engineered scaffolds that behave as microenvironments able to correctly guide cell functions and to provide, at the same time the essential structural support [1]. Such scaffolds should recapitulate the cell physiological surroundings, mimicking the topographical and biophysical cues that exist in natural extracellular matrix (ECM) and that significantly affect cell behavior [2-6]. Among the solutions adopted to build biocompatible ECM-like scaffolds [7-8] several techniques, including self-assembly, porogen-leaching, electrospinning, freeze-drying, phase separation, have been used to fabricate nano- or micro-scale fibrous scaffolds, reproducing the topographical architecture of native ECM [9-14]. For example, in bone tissue engineering scaffolds with a fiber-like structure could effectively promote cellular activity, recapitulating the fibrillar architecture of the bone ECM. To this aim, the electrospinning approach is mainly favored due to its versatility, simplicity and ease of scaling up: the morphology of the fibers, ranging from nano- to micro- scale, can be finely tuned by changing the processing parameters, such as the applied voltage, polymer concentration and collector distance [15-17]. Moreover, electrospun scaffolds display high porosity and a high surface area, besides the ECM-like nano-topography, thus promoting cell adhesion, spreading and proliferation [18]. Over the years, several natural and synthetic polymers have been exploited as electrospun substrates for bone regeneration. Among them, polycaprolactone (PCL), an already FDA-approved synthetic aliphatic polyester, has been extensively adopted because of its excellent biocompatibility and ease of manufacturing and processing [19-22]. However PCL does not promote cell adhesion and proliferation, due to its high hydrophobicity [23]; consequently many efforts have been carried out either to generate chemical modifications of the electrospun fibers or to produce co-

electrospun structures [24, 25], by combining PCL with other more bioactive species, such as inorganic nano-materials like hydroxyapatite [26], bio-silica [27], calcium carbonate [28], or carbon-derived nanomaterials [29, 30]. In particular, carbon nanomaterials have recently attracted the interest of the biomedical scientific community, owing to their excellent mechanical strength and tailorable surface properties [31, 32]. Graphene, which is a single layer of aromatic carbon atoms in a two–dimensional lattice can be synthetized in a relative pure form, preserving its unique mechanical, physical and chemical properties [33]. Once more, though, the hydrophobic nature of graphene calls for the generation of various derivatives to fabricate functional polymer composites. Among these, graphene oxide (GO) displays a higher dispersibility and hydrophilicity, conferred by the high number of available functional groups (e.g. hydroxyl, epoxide, and carbonyl ones) bound on its high surface area [34-37]. Previous studies have shown that cells successfully adhere and proliferate on GO substrates [38], including undifferentiated progenitor cells such as induced pluripotent stem cells (iPSCs), mesenchymal stem cells (MSCs) and neural stem cells (hNSCs) [39-43]. Electrospun polycaprolactone (PCL)/GO nano-fibrous scaffolds have also been proved to enhance the lineage commitment of undifferentiated PC12 and MSCs cells into neuro-like and osteo-like cells, respectively [44]. Nonetheless, since graphene oxide does not retain all the same features of the pristine graphene, reduced graphene oxide (RGO) [45, 46], obtained by a simple chemical reduction of GO [36], drew our attention. Indeed RGO displays different physical and chemical natures with respect to GO, peculiarly in terms of electrical activity and nano-topography [47]. Although some groups have realized GO-RGO composite polymeric fibrous scaffolds [44-48], the distinct effects of RGO incorporation on the bioactivity and biomineralization of fibrous mats have not been elucidated yet. Accordingly, in this work, we have finalized a new protocol to

realize RGO-functionalized polymeric electrospun fibers by using a bio-friendly versatile process. We have then extensively characterized the resulting nanofibrous scaffolds in terms of structural, chemical and biological properties *in vitro.* These last, in particular, have been investigated focusing on cell viability, spreading and proliferation of three different fibroblast or osteoblast-like cell lines. Then we have examined the *in vitro* mineralization of the matrix deposited by osteoblast-like cells and, ultimately, the mRNA transcript levels of osteogenic specific markers of MSC seeded onto RGO-incorporating membranes to evaluate their potential as substrates for bone tissue engineering.

2. Materials and Methods

2.1 Materials

Graphene oxide flakes (Sigma Aldrich, Product No. 763713) suspension (1 mg/ml) were prepared by ultrasonic treatment (FALC Instruments, LBS1) for 3 hours suspending 100 mg of graphene oxide in 100 ml of absolute ethanol (EtOH). Commercial graphene oxide was produced through oxidation/exfoliation of graphite powder via the modified Hummer's method. GO nanoflakes displayed mean lateral size of 6.28 ± 0.16 μm and mean thickness of 4.00 ± 0.28 nm. GO was reduced through L-Ascorbic Acid (L-AA, Sigma Aldrich, Product No. A5960) as previously reported [49]. Briefly, 10 mg of L-AA has been added to 1 ml of GO/EtOH dispersion (1mg/ml) and mixed for 48 hours under constant stirring.

To realize the graphene-based nanofibrous meshes, PCL (molecular weight = 45.000, Sigma Adrich, Product No. 704105) was dissolved in chloroform (CF) under stirring over night to obtain 40% w/v polymeric solution. Then the same volume of either GO/EtOH or RGO/EtOH was added to the PCL solution to obtain a 0.25 wt% GO-RGO/PCL composites solutions having 20% w/v PCL on total volume. As control, a PCL/CF 40% w/v solution was prepared, and mixed with an equal volume of EtOH to obtain a 20% w/v PCL solution in CF-EtOH.

2.3 Fabrication of PCL based fibrous scaffolds via Electrospinning

A custom-made electrospinning machine was used to prepare pure PCL- and GO-RGO/PCL-nanofibrous scaffolds. The polymeric mixtures were filled in a 6 ml plastic syringe fitted with a 21-gauge stainless steel needle. A syringe pump (PHD 2000, Harvard Apparatus) was set to guarantee a 2ml h^{-1} constant flow rate, while a constant voltage of 10 kV was supplied by a high voltage power supply (ES 50P-10W, Gamma high Voltage Research). The obtained nanofibers were collected on rectangular (75×25 mm^2) borosilicate glass coverslips, mounted on a grounded collector at a distance of 12 cm from the needle for 2 hours. The collected nanofibers were subsequently vacuum dried for 24 hours. The air relative humidity and temperature conditions were about 40% and 23°C, respectively. As control, the same solutions were employed to obtain planar films. At the end of the procedure, six different samples were available: PCL, GO/PCL and RGO/PCL, all as nano-fibrous structures or films. All samples were washed three times in PBS for 15 minutes, followed by one additional over night rinse in EtOH 70% and sterilized by UV irradiation before cell culture.

2.4 Scaffold characterization

The morphology of nano-fibrous samples was analyzed by scanning electron microscopy (SEM): NFs were imaged by a Raith 150 system (Raith, Dortmund, Germany) using an accelerating voltage of 5 kV and an aperture size of 20 µm. No metal was deposited on samples before SEM, to better evidence the embedded nanocrystals. The average porosity (P) of fibers mats, the average fiber diameter as well as the average fiber orientation were calculated through Image J® software from binarized SEM images. In particular, P was assessed through a semi-automatic image post-processing of binarized images, by calculating the ratio between the number of pixels representing the voids and the total number of pixels of the images. The average thickness of the fibers was calculated by using the tool "Thickness" of the open source plugin "BoneJ", which returns a coloured map of the thickness of the fibers and the histogram of the diameter distribution. The average orientation of the fibers was evaluated through the plugin "OrientationJ" developed for directional analysis, its outputs are a visual representation of the fibers orientations through a coloured map and a quantitative assessment of the distribution of the fibers orientation.

All the measurements were carried out in triplicate for each category of samples.

The local surface morphology and the root mean square roughness (σ_{RMS}) of GO/PCL and RGO/PCL film were carried out by using a TT-AFM (AFMWorkshop, Signal Hill, CA, USA) equipped with 50x50 µm^2 scanner. All the measurements were performed in contact mode, in air at room temperature by using rectangular silicon cantilevers (model CSG01, NT-MDT & Co., Moscow, Russia) with a spring constant of 0.03 N/m and with a nominal tip radius of 10 nm. Topography images, of 15 x 15 µm size, were acquired at a resolution of 512 pixels per line using a scan rate of 1 Hz. AFM scanner performance and calibration was routinely checked by

using a reference square grid, model SHS-0.1-1 (AppNano, Santa Clara, CA, U.S.A.) with a lateral pitch of 3μm and step height of 104 nm. Imaging was performed several times on different points per samples. AFM images were pre-processed for tilt correction and scars removal with Gwyddion software.

The surface roughness for an AFM image is described by root mean square roughness (σ_{RMS}) calculated according to the following equation:

$$\sigma_{RMS} = \sqrt{\frac{1}{N}\sum_{i=1}^{N}(Z_i - Z)^2}$$

where N is the number of pixels of the image, Z_i is the height of each pixel and Z is the mean height. The surface roughness was estimated by AFM height data as the average value over 19 different places on the surface for each sample.

The presence of nano-sheets and the resulting chemical composition of nano-fibrous mats were analyzed by Fourier-transform infrared (FTIR) spectroscopy (OMNIC™ software, DTGS detector) in transmission mode. Spectra were recorded in the 450–4000 cm^{-1} range with 256 scans at spectral resolution of 2 cm^{-1}, averaged and baseline-corrected. FTIR skeletal spectra of PCL, GO/PCL and RGO/PCL nanofibers mats were carried out on dish obtained after grinding the sample in an agate mortar with KBr powder (Aldrich, FT-IR grade) (1%, w/w). GO and RGO were analyzed by spreading the corresponding EtOH liquid dispersions on a KBr dish and then drying the samples in vacuum. FTIR analyses were performed with Nicolet Nexus Fourier transform instrument (OMNIC™ software, DTGS detector).

Mechanical loading tests were performed on the electrospun meshes in the axial direction using a uniaxial Z0.5 test machine (Zwick Roell, Ulm, Germany). Each sample (n = 5 specimens) was cut into rectangular shapes (30 mm×10 mm) with a thickness of 0.1 mm. The thickness of each sample was measured using a digital caliper (Series 209, Mitutoyo, USA). Every segment was clamped with screw grips at its cut ends. All the tests were performed at constant velocity, set at 20 mm/min, with a preload of 0.1 N. Young's modulus was calculated from the slope of the best-fitting straight line, stress vs. strain, in the range 3-5 % of the strain.

Statistical analysis was assessed using a Student's paired t-test. Statistical significance was considered at $P < 0.005$.

2.5 Cell viability and morphology

Mouse fibroblast cell line (NIH-3T3) was expanded in a Dulbecco's Modified Eagle's Medium (DMEM) supplemented with 10% fetal bovine serum (FBS) and 1% (v/v) penicillin/streptomycin. The culture media was changed twice a week. At confluence, 3T3 cells were enzymatically detached with 0.05 % trypsin and counted.

Cells were seeded onto the fibers mats and films at a density of 4×10^4 cells for sample and cultured for 24 hours. Cell viability was evaluated through a live/dead assay (Sigma Aldrich). Briefly, samples were washed with PBS and incubated in 2mM calcein AM and in 4mM EthD-1 in PBS for 15 min at 37°C in the dark, to detect live and dead cells, respectively. Cells were then rinsed in PBS again. Positivity to either staining solution was observed by means of fluorescence microscopy (Nikon H550L).

Cell spreading and morphology were evaluated through toluidine blue staining and SEM analysis. The samples were washed in buffer saline solution and fixed in paraformaldehyde 3.7% for 1 hour. Then they were rinsed in PBS to remove the paraformaldehyde excess and dehydrated with a series of concentration-increasing ethanol solutions. After drying for 24 hours, the samples were stained with toluidine blue and observed with an optical microscope (Nikon H550L).

For SEM analysis, the samples were dehydrated, as described above, dried for 24 hours, and coated with a gold film before observation with a scanning electron microscope using a Hitachi S-2500, to evaluate cells adhesion and spreading. All experiments were performed in triplicate.

2.6 Cell Proliferation

For the biological validation of the developed materials, we used different cell systems, i.e. a mouse fibroblast cell line (NIH-3T3) and two human osteosarcoma cell lines (HOS and MG-63). Cells were expanded in a Dulbecco's Modified Eagle's complete medium (DMEM) supplemented with 10% fetal bovine serum (FBS) and 1% (v/v) penicillin/streptomycin. Culture media was changed twice a week. At confluence, cells were enzymatically detached with 0.05 % trypsin and counted.

Cells were seeded onto the fibers mats and film at a density of $4x10^4$ cells for sample and cultured up to 1 week. Cell proliferation was assessed using Presto Blue Assay (Thermo Fisher Scientific). In brief, after one (T1), four (T4) and seven (T7) days the medium was removed from all samples and replaced with fresh medium containing 1% v/v of Presto Blue solution, as indicated. Samples were incubated at 37°C for 45 minutes in dark. The supernatants were

collected and absorbance readings at 570 and 600 nm assessed spectrophotometrically. Proliferation rate was defined as number of alive cells at different time points normalized respect to the number of cells alive after few hours from the seeding. Data were analyzed by the Student's paired t-test (*n=9*). Statistical significance was set at p < 0.05.

2.7 Adsorption of osteogenic factors

Adsorption of soluble osteogenic factors on fibrous membranes was evaluated in accordance with the literature with slight modifications [50]. Dexamethasone (10mM), β-Glycerolphosphate (1M), and Ascorbic Acid (10mM) solutions (all purchased from Sigma Aldrich) were prepared separately in DI water. PCL, GO/PCL and RGO/PCL composite fibrous meshes were incubated with each solution for 3 days at 37 °C. The adsorption of the chemicals was evaluated with UV-Vis spectroscopy by sampling the surnatants of the incubated materials confronting the absorbance with the original solutions in the wavelength range of 200–250 nm. Data were analyzed by the Student's paired t-test (*n=5*). Statistical significance was set at p < 0.05.

2.8 Biomineralization

HOS cells were seeded onto the fibers mats at a density of $5x10^4$ cells for sample. After 24 hours, the samples were rinsed with osteogenic medium, which consisted of complete medium supplemented with 0.2 mM Ascorbic Acid and 10 mM β-Glycerophosphate and 10^{-8} M Dexametasone.

Calcium mineralization was determined by Alizarin red staining of HOS cells after 14 days of culture. PCL, GO/PCL and RGO/PCL electrospun membranes were washed three times with PBS and fixed with 4% w/v formaldeide. Upon three additional washes in DI water they were stained with alizarin red (40mM, pH: 4.1-4.3) for 20 min at room temperature. After several washes with DI water, the mats were observed under optical microscope (Nikon H550L).

2.9 mRNA extraction and gene expression analysis

Commercially available human mesenchymal stromal cells (MSC; Lonza; Walkersville, MD, USA) were expanded in Coon's-modified Ham's F12 medium (Biochrom A.G., Berlin, Germany), supplemented with 10% FBS and with 10 ng/mL Fibroblast Growth factor-2. At confluence, MSC osteoinduction was carried out by substituting the standard culture medium with a differentiation-factor enriched one (F12 medium supplemented with 10% FBS, 2.5×10^{-4} M Ascorbic acid, 1.0×10^{-2} M β-Glycerophosphate, 1.0×10^{-7} M Dexamethasone) as previously indicated [51]. Osteoinduced MSC were then detached by tripsinization, counted and used to extract total mRNA by means of the PerfectPure RNA Cultured Cell Kit (5-Prime GmbH, Hamburg, Germany), according to the manufacturer's instructions. Concentration and purity of the extracted mRNAs were assessed spectrophotometrically at 260/280 nm. For each sample the corresponding cDNA pool was generated using the SuperScript^{TM} III First-strand synthesis system for RT-PCR Kit (Invitrogen, Milano, Italy). Primer sets for each gene (glyceraldehyde-3-phosphate dehydrogenase, (GAPDH), Runx2, Osteopontin (OP), Osteocalcin (OC), Bone Sialoprotein I (BSP), were derived from previously published sequences [52]. The expression of target genes was assessed by sybr-green real time quantitative RT-PCR in an Eppendorf Mastecycler Realplex^2 apparatus; the cDNAs were amplified with the RealMasterMix SYBR ROX 2.5X (5'-Prime), performing quadruplicate reactions for each sample, according to the following protocol: 95°C for 3 minutes; 35 cycles at 94°C for 30 sec, 60°C for 30 sec, 72°C for 40 sec, and a final step at 72°C for 7 min. Gene expression, in each sample, was normalized to the endogenous housekeeping gene GAPDH. The resulting expression ratio was normalized versus the same ratio obtained in osteogenicaly-induced hMSC cultured on plastic. The melting

curve analysis was used to countercheck the unicity of the amplified products. Data were analyzed by the Student's paired t-test ($n=4$). Statistical significance was set at $p < 0.05$.

3. Results and Discussion

3.1 Scaffold characterization

Figure 1 shows ethanol and the homogeneous GO and RGO solutions in ethanol before electrospinning (panels A, B, C respectively), SEM images of PCL, GO-PCL, RGO-PCL electrospun fibrous meshes at different magnifications (panels D-I), and their morphological analysis (panels L-N). Conventional fabrication methods used to reduce GO typically require extreme pH solutions, toxic reducing agents, such as hydrazine, making the final materials incompatible with cellular studies. The organic compound L-Ascorbic acid, also known as Vitamin C, is a natural anti oxidant and can act as reducing agent of many reactive oxygen species.

In this work, we have adapted an already established protocol for the L-AA-based reduction of GO [49] to provide an efficient and non-toxic method to realize RGO/PCL substrates.

After 48 hours of L-AA incubation with GO nanosheets, color changes of the GO solution occured, from brown to black, confirming the reduction reaction (Figure 1, B-C), in agreement with data reported in the literature [49].
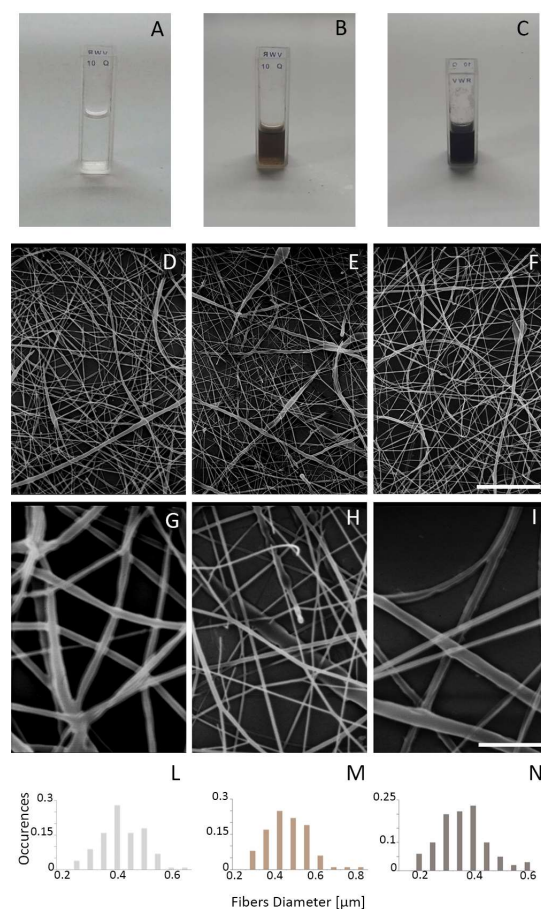
Figure 1. Photographs of typical EtOH (A), GO (B), RGO (C) solutions (1 mg/ml GO-RGO/EtOH; SEM microscope images of PCL (panels D, G), GO/PCL (panels E, H), RGO/PCL (panels F, I) nanofibers mesh. Scale bars: 24 μm (panels D-F); 5 μm (panels G-I); occurrence of fiber distribution, according to their diameter, expressed in microns, for PCL (panel L), GO/PCL (panel M), RGO/PCL (panel N) nanofibers mesh.

The three categories of fibrous materials hereby introduced (PCL, GO/PCL, RGO/PCL) displayed a similar morphology (Figure 1, D-I); in particular, the fibers were randomly oriented and showed a three-dimensional open porous structure. The average diameters of the fibers and the overall porosity were not affected by the graphene nano-sheets introduction by any statistical relevance ($p > 0.005$).

	Fibers Average Diameter	Porosity (%)
PCL	380 nm ±100 nm	89.45 ±7.43
GO/PCL	430 nm ±110 nm	95.05 ±9.73
RGO/PCL	410 nm ±115 nm	92.47 ±4.12

Table 1. Average diameter and porosity values for PCL, GO/PCL, RGO/PCL electrospun nanofibers.

The incorporation of graphene nanocomposites derivatives can induce variation of surface roughness at the nanoscale level, contributing well to the substrate heterogeneous nanotopography. As a result, it may be able to influence the cell anchorage and growth. To evaluate this hypothesis, we investigated the surface coverage and roughness in the GO/RGO–PCL nanocomposites.

Analysis of AFM images (Figure 2) of GO/PCL and RGO/PCL films showed an increased membrane roughness, confirmed by measures of σ_{RMS} being 96 nm ±16 and 202 nm ±65 respectively, highlighting an higher nanoscale roughness ($p<0.005$) in the polymeric mesh functionalized with RGO. These results are also in agreement with some studies showing a different roughness between GO and RGO flakes [47], and in particular a greater roughness in ascorbic acid reduced RGO monolayers when compared to the GO monolayer [53].
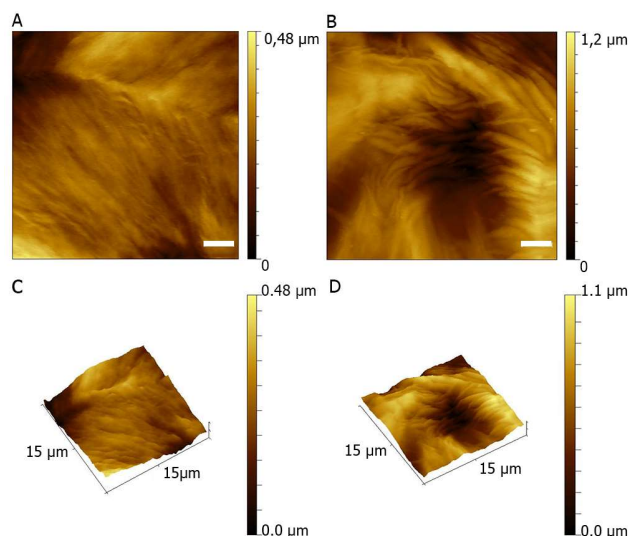
Figure 2. AFM images of GO/PCL (Panels A, C) and RGO/PCL (Panels B, D) substrates. Scale bars: 2 μm.

A chemical interaction between PCL chains and GO/RGO with the formation of hydrogen bonds was displayed through the FTIR analysis (Figure 3), as reported by the reduction of the intensity of -OH groups (broad peak at 3400 cm^{-1}) in GO/PCL and RGO/PCL with respect to PCL. The enduring broad peak at 3400 cm^{-1} in the FTIR spectrum of RGO was due to the moisture contained in the KBr dish which could not be avoided [54]. Moreover, a reduction of the ratio n_{1730} / $n_{1250-1100}$, corresponding to vCO and vC-C respectively, was observed for the GO/PCL samples in comparison with PCL ones, while the ratio reduction was not observed in the RGO/PCL samples; this result could suggest a chemical interaction among the polymeric chains and the GO molecules, although no shifting of the peaks in the range 1200-1000 cm^{-1} was observed in PCL and GO/PCL samples. Lastly, no peak relative to ascorbic acid was detected in the RGO/PCL spectrum.
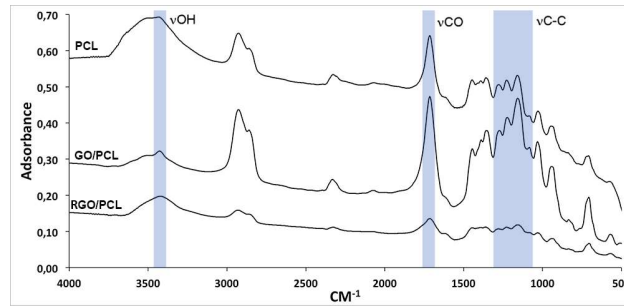
Figure 3. FTIR spectra of PCL, GO/PCL, RGO/PCL nanofibers meshes.

The mechanical performances of nano-fibrous mats were evaluated through loading tests. The PCL alone behaves like a semi-crystalline and ductile polymer and the addition of GO and RGO nano-sheets to the fibrous meshes did not significantly affect this feature; however, it enhanced the mechanical performance. In particular, the Young's modulus changes from 1.51 ±0.18 MPa for PCL to 1.85 ±0.23 MPa with the incorporation of GO and to 2.09 MPa with RGO, with an increase of a 22% and 38%, respectively. This effect was coupled with a strength increase, in particular for PCL nanofibrous meshes we observed a tensile strength of 0.25 MPa, while we obtained values of 0.37 ±0.03 MPa for GO/PCL and 0.29 ±0.034 MPa for RGO/PCL, therefore with an increase of 45% and 14%, respectively.

Our findings keep in line with the current literature, where sensible increments of the mechanical proprieties of electrospun nanofibers were proved, subsequently to the addition of small amount of graphene-derived nanomaterials [23, 55]. An increase in the mechanical properties of PCL nanofibers in the presence of GO and RGO nanosheets is attributed to the adhesion between nanosheets and PCL matrix [56]. The higher stiffness of the GO/PCL specimens with respect to the PCL ones may be cross-correlated with the chemical interaction between the PCL chains and the GO sheets, shown by FTIR spectra. On contrary, no chemical bonds between RGO and PCL were detected, therefore the enhancement of the mechanical properties may be due to the

enhanced roughness of RGO/PCL that could lead to the consequent reduction of the sliding motion among the fibers in the mats.

In particular, at microstructural level, the stiffness of a polymeric substrate is connected with the motility and flexibility of its organic chains [55]. In particular, the introduction of particles increases the stiffness of an organic matrix because of a reduction of the flexibility of the polymeric chains. This phenomenon occurs also without the formation of new chemical bonds among the polymeric matrix and the particles, as a result of their steric encumbrance [56].

Based on our results, we hypothesize that the rougher surface of RGO/PCL substrates at the nanoscale level, shown by AFM analysis, finally contributes to an higher Young's Modulus of RGO/PCL substrates, if compared with GO ones. Therefore, in our experimental case, the topographical/physical features conferred by RGO addition seem to provide a larger contribution to an enhanced stiffness than the chemical interactions driven by the presence of GO.

3.2 Cell viability, spreading and proliferation

The cell viability, spreading and proliferation on the electrospun nanofibers mats were investigated to evaluate whether the GO/RGO incorporated PCL nanofibrous mats are fundamentally suitable for tissue engineering approaches, and how the addition of graphene derivatives played a role in cell recognition of, adhesion to and compatibility with a given substrate.

It is evident from Figure 4A that the amount of cells alive onto the polymeric substrates was higher in the graphene-incorporating nanomaterials, and more evident in the presence of RGO than of GO.
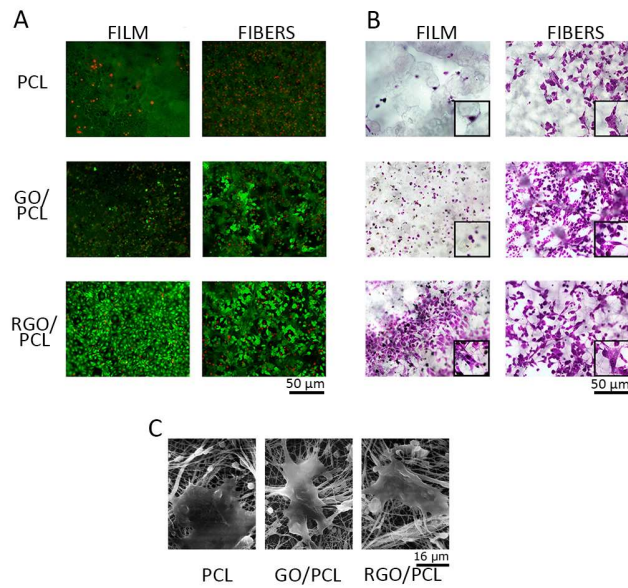
Figure 4. Fluorescent images (green spots: alive cells; red spots: dead ones) representing cell viability (panel A) and toluidine blue staining showing cell spreading (panel B) of 3T3s after 24 hours of culture on PCL-, GO/PCL- or RGO/PCL-based materials, the latter two generated as planar films (sheets, thin layers?). SEM images of 3T3s adhering to PCL-, GO/PCL-, RGO/PCL-electrospun nanofiber meshes after 24 hours of culture (panel C).

Moreover, an enhancement of the 3T3 cells spreading was observed on the polymeric substrates enriched with graphene oxide, even more evidently in samples doped with reduced graphene oxide (Figure 4B). In general, though, all nano-fibrous structured materials positively contributed to cell spreading. This keeps in line with what already reported in the literature [17], where nano-microfibers are described as a helpful architecture for cell adhesion. The improved viability and spreading of cells cultured onto nanofibrous graphene derivates/PCL meshes indicate that topography (at the micro-scale) and roughness (at the nano-scale) significantly stimulate cell adhesion and proliferation. These results are also partially in agreement with previous reports showing a higher cell proliferation in the presence of graphene oxide (GO), possibly due to an increased protein adsorption on GO surfaces [18, 57], which would facilitate the adhesion role of cell surface determinants.

However, up to now, no studies have reported and described the cell behavior onto fibrous

meshes doped with RGO in comparison with GO. Here, we show a significantly stronger cell spreading in RGO/PCL substrates than in GO/PCL or in PCL-only based ones.

SEM images showed 3T3s adhesion on PCL, GO/PCL and RGO/PCL nano-fibrous mats, respectively (Figure 4C). Cells growing on fibrous materials interacted strongly with the substrate and formed anchorage links via pseudopodia, owing to the porous structure and to the diameter of the fibers, overall reproducing the topographical structure of natural ECM. The fibrous substrates, therefore, well mimicked the cell native extracellular environment, facilitating cell attachment and proliferation. Indeed this aspect is of relevance, since it is widely accepted that an enhanced cell spreading and an eased cell–to-cell or cell–to-substrate interaction affect the cellular fate and maturation, particularly in progenitor mesenchymal cells [17]. Many studies have demonstrated that nano-micro-scale structures in bio-based materials provide advantages in inducing a positive cell response [11, 58]. The rougher surface of RGO-based materials, with respect to the GO-based ones, as shown by AFM analysis, can explain the enhanced cell spreading observed, since a larger surface area becomes available and suitable for cell attachment [59, 60].

Cell proliferation on PCL, GO/PCL and RGO/PCL nano-fibrous mats and planar films was continuously observed and quantified at 1, 4 and 7 days by using different cells lines (Figure 5): all samples showed a time-dependent proliferation of the cells after their adhesion to the surfaces (films or fiber meshes). In particular, the cell lines used, either of murine (3T3) or human (HOS, MG-63) origin, showed an increased proliferation with the introduction of carbon-derived nanomaterials, in particular with RGO ($p<0.005$), both in fibrous and film composites, indicating that RGO-PCL substrates may provide a more suitable environment for the proliferation of cells of mesenchymal origin.
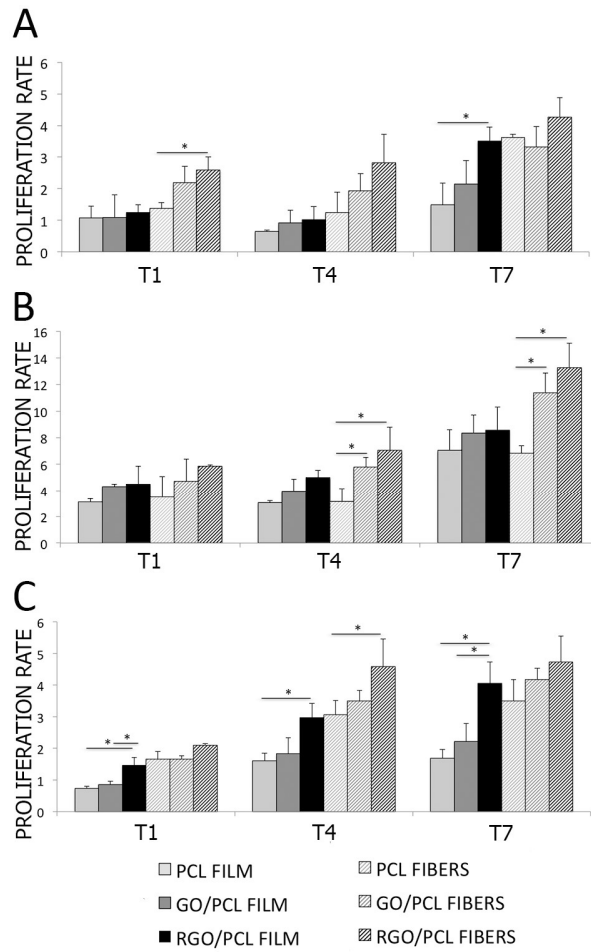
Figure 5. Proliferation rate of 3T3 (panel A), HOS (panel B) and MG-63 (panel C) cell lines up to one week of cell culture on PCL, GO/PCL, RGO/PCL based materials both as planar film or fibrous mats.

3.3 Adsorption of osteogenic factors

We further evaluated the role of GO and RGO, respectively, on the absorption of osteogenic growth factors. Previous studies have in fact shown that local availability of osteogenic factors may directly influence the differentiation of nearby cells [50, 61] and that graphene-based materials have the ability to adsorb biomolecules on their surface, due to the weak chemical

interactions and high surface area [62, 63].

Table 2 shows the normalized average concentrations of dexametasone, β-glycerol phosphate and ascorbic acid adsorbed onto GO- and RGO-based electrospun membranes, normalized with respect to PCL-based ones; for all the tested chemicals, adsorption onto GO/PCL- and RGO/PCL-meshes was markedly higher than onto PCL-only ones ($p < 0.005$). On the contrary, no significant difference was detected among the concentrations of growth factors adsorbed onto GO- and RGO-based substrates.

	Dexamethasone	β-Glycerol Phosphate	Ascorbic Acid
GO/PCL	1.8 ± 0.10	2.99 ± 0.09	1.91 ± 0.07
RGO/PCL	1.9 ± 0.12	3.66 ± 0.48	1.99 ± 0.03

Table 2. Normalized averages of the concentrations of the adsorbed osteogenic factors on GO/PCL and RGO/PCL electrospun meshes; values are the average ratio over the corresponding PCL values.

3.4 Biomineralization

The evaluation of ECM mineralization is the more effective *in vitro* analysis to assess the capability of a material to support cell osteogenic differentiation [64]. Alizarin red S staining over the electrospun meshes after 14 days of culture has been performed to evaluate the *in vitro* calcium deposition by HOS cells on the neo-deposited extracellular matrix during culture. Figure 6 shows the optical microscopic images of the staining, performed for PCL, GO/PCL, RGO/PCL fibrous mats in duplicate. A faint initial positive staining can be observed for PCL electrospun meshes, while clear red mineral deposits can be observed over GO-RGO/PCL based materials. Comparing GO and RGO-based substrates, a higher amount of mineralization can be observed for RGO/PCL fibrous mats.

The deposition of calcium phosphate in the ECM is a reflection of the osteogenic commitment of the cells and is suggestive of a potential use of these materials for bone tissue engineering applications.
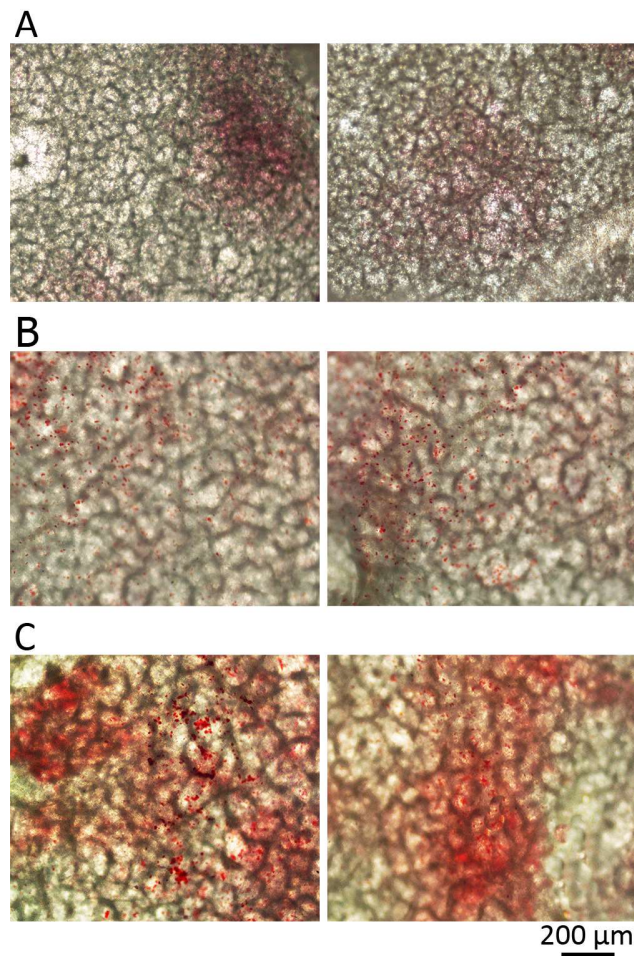
Figure 6. Alizarin red staining showing calcium deposition (in red) of HOS cultured in osteogenic medium for 14 days over PCL (Panel A), GO/PCL (Panel B), RGO/PCL (Panel C) electrospun-nanofibers meshes.

Material surface properties, such as topography, play a key role in cell growth and differentiation, which is well acknowledged in the literature [65, 66]: in particular, the higher the roughness of a solid substrate, the larger is the availability of nucleation sites for its

mineralization [67]. In this respect, AFM analysis has shown a σ_{RMS} of 202 nm ±65 and of 96 nm ±16 in RGO- and GO-enriched PCL meshes, respectively (p<0.05), suggesting that RGO-ones may represent a more favorable surface to biomineralization [68, 69]. Roughness, therefore, could be accounted for the different amount of calcium deposition observed among GO- and RGO-based electrospun meshes, even if the growth factors absorption analysis did not highlight any substantial difference between GO- and RGO- based substrates.

3.5 Influence of the RGO-doping of PCL-nano-fibrous mats on the expression of osteogenic differentiation markers in cultured human MSC

Based on the results observed so far, and in the attempt to mimic an applicative scenario of the nano-fibrous mats, we osteoinduced cultured human MSC over RGO/PCL and PCL fibrous meshes and evaluated the expression of osteogenic differentiation marker genes, such as RUNX2, Osteocalcin (OC), Osteopontin (OP) and Bone Sialoprotein (BSP) (Figure 7). In spite of the fact that these progenitor cells are forced to differentiate in the absence of a physiological ECM and devoid of any vascularization (*i.e.* in a rather hostile environment), the nano-fibrous characteristics of the mats surfaces are sufficient to differently enhance the cell response. In fact RUNX2, a master transcription factor for osteogenic differentiation, remains upregulated in RGO-cultured cells (Figure 7A), and its overexpression can be held responsible for the downstream enhancement of Osteocalcin and BSP mRNAs [70, 71] (Figure 7, B-C). Indeed an enhanced expression of specific proteins is a pre-requisite for matrix deposition and mineralization: this is the case for BSP, which is a nucleator of matrix mineralization and plays a major role in osteointegration and vascular invasion of the newly deposited bone matrix [72], and for OP (Figure 7D), an abundant non-collagenous protein which accumulates at the

interfaces of cells and matrix in bone and contributes to mineralization and remodeling metabolism [73]. The detected relative but concordant increased levels of transcripts for all those aforementioned osteogenic markers found in RGO-cultured cells, then, may sustain an increased expression of those proteins necessary to generate an enhanced mineralization, as also concomitantly evidenced by Alizarine-staining in RGO-cultured HOS cells.
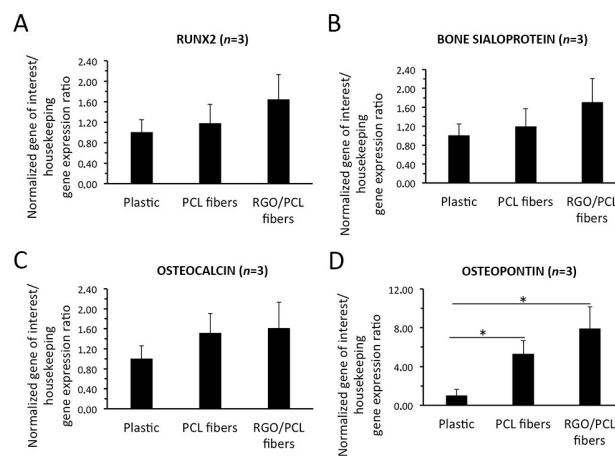
Figure 7. Normalized mRNA levels of osteogenic markers in MSC cultured onto different substrates. The histograms depict the average ratio of the expression levels for each gene of interest (RUNX2, Osteocalcin, Osteopontin or Bone Sialoprotein (BSP)) over the corresponding glyceraldehyde-3-phosphate dehydrogenase (GAPDH) level, in each culture condition (plastic, PCL fibers or RGO/PCL electrospun meshes). Average values are normalized versus the standard culturing condition (plastic). Error bars depict standard deviation ($n=4$).

As a whole, then, collected data indicate that RGO/PCL electrospun nanofibers, more properly than GO/PCL ones, enhance the triggering of the mineralization cascade of the neo-deposited matrix and may promote the osteogenic commitment of the cultured cell in the surrounding microenvironment, owing to a synergic action of the absorbed factors and of an increased surface roughness.

5. Conclusions

Biocompatible GO/PCL and RGO/PCL composite nano-fibrous mats have been successfully developed by elettrospinning. We have provided a new methodology based on the biological ascorbic acid compound to reduce GO to RGO and manufacture RGO/PCL fibrous composites. The morphological properties in terms of porosity and fiber diameter are not modified with the introduction of the nanomaterial. Despite the low amount of GO/RGO doping, a 22% and 38% enhancement of the Young's modulus and 45% and 14% of the tensile strength, was shown for GO/PCL and RGO/PCL nanofibers mats, respectively. This different biomechanical behavior can be explained by the different topographical features of the two graphene-derived composite substrates: AFM analysis revealed that RGO-based materials have a rougher surface at the nanoscale level, leading to a consequent reduction of the sliding motion among the fibers of the mats. Although both GO- and RGO-functionalized nanofiber mats showed a high biocompatibility, RGO-based substrates were more efficient in improving cell viability, spreading and proliferation rate, as assessed with different cell lines. Furthermore, RGO/PCL electrospun meshes induced enhanced *in vitro* calcium deposition and increased expression of genes involved in ECM mineralization in osteogenically induced cultured cells as a consequence of their surface chemical and topographical features. Perspectively, therefore, the generation of RGO-doped fibrous PCL scaffolds may provide a bioactive 3D-matrix with nano- to micro-scale typical cues favorable for bone tissue engineering applications.

Conflicts of Interests

There are no conflicts to declare

References

1. S. Yang, K.-F. Leong, Z. Du and C.-K. Chua, *Tissue Eng.*, 2001, 7, 679-689.
2. C. Liu, Z. Han and J. T. Czernuszka, *Acta Biomater.*, 2009, 5, 661-669.
3. G. Pennesi, S. Scaglione, P. Giannoni and R. Quarto, *Curr. Pharm. Biotechnol.*, 2011, 12, 151-159.
4. T. Sun, G. Qing, B. Su and L. Jiang, *Chem. Soc. Rev.*, 2011, 40, 2909-2921.
5. N. J. Sniadecki, R. A. Desai, S. A. Ruiz and C. S. Chen, *Ann. Biomed. Eng.*, 2006, 34, 59-74.
6. C. X. Guo, X. T. Zheng, Z. S. Lu, X. W. Lou and C. M. Li, *Adv. Mat.,* 2010, 22, 5164-5167.
7. C. Chen, T. Zhang, Q. Zhang, X. Chen, C. Zhu, Y. Xu, J. Yang, J. Liu and D. Sun, *ACS Appl. Mater. interfaces*, 2016, 8, 10183-10192.
8. S. Shah, P. T. Yin, T. M. Uehara, S. T. D. Chueng, L. Yang and K. B. Lee, *Adv. Mater.*, 2014, 26, 3673-3680.
9. Z.-M. Huang, Y.-Z. Zhang, M. Kotaki and S. Ramakrishna, *Compos. Sci. Technol.*, 2003, 63, 2223-2253.
10. W. J. Li, C. T. Laurencin, E. J. Caterson, R. S. Tuan and F. K. Ko, *J. Biomed. Mater. Res.*, 2002, 60, 613-621.
11. G. Wei and P. X. Ma, *Adv. Function. Mat.*, 2008, 18, 3568-3582.
12. M. Shin, H. Yoshimoto and J. P. Vacanti, *Tissue Eng.*, 2004, 10, 33-41.
13. A. Marrella, M. Aiello, R. Quarto and S. Scaglione, *Biotecnol. Bioeng.*, 2016, 113, 2286-2297.
14 A. Marrella, A. Lagazzo, E. Dellacasa, C. Pasquini, E. Finocchio, F. Barberis, L. Pastorino, P. Giannoni and S. Scaglione, *Polymers*, 2018, 10, 380.
15. D. H. Reneker and I. Chun, *Nanotechnology*, 1996, 7, 216.
16. C. P. Barnes, S. A. Sell, E. D. Boland, D. G. Simpson and G. L. Bowlin, *Adv. Drug Deliv. Rev.*, 2007, 59, 1413-1433.
17. A. Polini, D. Pisignano, M. Parodi, R. Quarto and S. Scaglione, *PloS one*, 2011, 6, e26211.
18. W. Shao, J. He, Q. Han, F. Sang, Q. Wang, L. Chen, S. Cui and B. Ding, *Mater. Sci. Eng. C*, 2016, 67, 599-610.
19. J. H. Jang, O. Castano and H. W. Kim, *Adv. Drug Deliv. Rev.,* 2009, 61, 1065-1083.
20. G. Ciapetti, L. Ambrosio, L. Savarino, D. Granchi, E. Cenni, N. Baldini, S. Pagani, S. Guizzardi, F. Causa and A. Giunti, *Biomaterials*, 2003, 24, 3815-3824.
21. M. A. Woodruff and D. W. Hutmacher, *Progr. Polym. Sci.* 2010, 35, 1217-1256.

22. E. Alarçin, T. Y. Lee, S. Karuthedom, M. Mohammadi, M. A. Brennan, D. H. Lee, A. Marrella, J. Zhang, D. Syla, Y. S. Zhang, A. Khademhosseini and H. L. Jang, *Biomer. Sci.,* 2018.
23. C. Wan and B. Chen, *Biomed. Mater.* 2011, 6, 055010.
24. M. A. Alvarez-Perez, V. Guarino, V. Cirillo and L. Ambrosio, *Biomacromolecules*, 2010, 11, 2238-2246.
25. L. Ghasemi-Mobarakeh, M. P. Prabhakaran, M. Morshed, M.-H. Nasr-Esfahani and S. Ramakrishna, *Biomaterials*, 2008, 29, 4532-4539.
26. Z. Su, J. Li, Z. Ouyang, M. M. Arras, G. Wei and K. D. Jandt, *RSC Adv.*, 2014, 4, 14833-14839.
27. W. E. Müller, E. Tolba, H. C. Schröder, B. Diehl‐Seifert, T. Link and X. Wang, *Biotechnol. J.* 2014, 9, 1312-1321.
28. K. Fujihara, M. Kotaki and S. Ramakrishna, *Biomaterials*, 2005, 26, 4139-4147.
29. K. Saeed, S. Y. Park, H. J. Lee, J. B. Baek and W.-S. Huh, *Polymer*, 2006, 47, 8019-8025.
30. Z. Meng, W. Zheng, L. Li and Y. Zheng, *Mater. Sci. Eng. C*, 2010, 30, 1014-1021.
31. M. Kalbacova, A. Broz, J. Kong and M. Kalbac, *Carbon*, 2010, 48, 4323-4329.
32. O. Im, J. Li, M. Wang, L. G. Zhang and M. Keidar, *Int. J. Nanomedicine*, 2012, 7, 2087-2099.
33. S. Stankovich, D. A. Dikin, G. H. Dommett, K. M. Kohlhaas, E. J. Zimney, E. A. Stach, R. D. Piner, S. T. Nguyen and R. S. Ruoff, *Nature*, 2006, 442, 282-286.
34. H. Chen, M. B. Müller, K. J. Gilmore, G. G. Wallace and D. Li, *Adv. Mat.*, 2008, 20, 3557-3561.
35. J. Kim, L. J. Cote, F. Kim, W. Yuan, K. R. Shull and J. Huang, *J. Am. Chem. Soc.,* 2010, 132, 8180-8186.
36. D. R. Dreyer, S. Park, C. W. Bielawski and R. S. Ruoff, *Chem. Soc. Rev.*, 2010, 39, 228-240.
37. C. Chung, Y.-K. Kim, D. Shin, S.-R. Ryoo, B. H. Hong and D.-H. Min, *Accounts Chem. Res.,* 2013, 46, 2211-2224.
38. G. Y. Chen, D. W. Pang, S. M. Hwang, H. Y. Tuan and Y. C. Hu, *Biomaterials*, 2012, 33, 418-427.
39. S. H. Ku and C. B. Park, *Biomaterials*, 2013, 34, 2017-2023.
40. B. Chaudhuri, D. Bhadra, L. Moroni and K. Pramanik, *Biofabrication*, 2015, 7, 015009.
41. D. Depan, B. Girase, J. Shah and R. Misra, *Acta Biomater.*, 2011, 7, 3432-3445.
42. A. Solanki, S. T. Chueng, P. T. Yin, R. Kappera, M. Chhowalla and K. B. Lee, *Adv. Mat.,* 2013, 25, 5477-5482.
43. A. Marrella, A. Lagazzo, F. Barberis, T. Catelani, R. Quarto and S. Scaglione, *Carbon*, 2017, 115, 608-616.
44. J. Song, H. Gao, G. Zhu, X. Cao, X. Shi and Y. Wang, *Carbon*, 2015, 95, 1039-1050.
45. O. Akhavan, E. Ghaderi, E. Abouei, S. Hatamie and E. Ghasemi, *Carbon*, 2014, 66, 395-406.
46. X. Shi, H. Chang, S. Chen, C. Lai, A. Khademhosseini and H. Wu, *Adv. Funct. Mat.*, 2012, 22, 751-759.
47. I. Kanayama, H. Miyaji, H. Takita, E. Nishida, M. Tsuji, B. Fugetsu, L. Sun, K. Inoue, A. Ibara, T. Akasaka, T. Sugaya and M. Kawanami, *Int. J. Nanomedicine*, 2014, 9, 3363-3373.

48.   S. Ramazani and M. Karimi, *Materials Science and Engineering: C*, 2015, 56, 325-334.
49.   J. Zhang, H. Yang, G. Shen, P. Cheng, J. Zhang and S. Guo, *Chem. Comm.*, 2010, 46, 1112-1114.
50.   W. Qi, W. Yuan, J. Yan, H. Wang, *J. Mater. Chem. B*, 2014, *2*, 5461-5467.
51.   G. Shyti, F. Rosalbino, D. Macciò, L. Scarabelli, R. Quarto and P. Giannoni, *Int. J. Artif. Organs*, 2013, *37*, 149-164.
52.   P. Giannoni, F. Villa, C. Cordazzo, L. Zardi, P. Fattori, R. Quarto, M. Fiorini, *Biomater. Sci.*, 2016, 4, 1691-1703.
53.   S. Eigler, S. Grimm, M. Enzelberger-Heim, P. Müller and A. Hirsch, *Chem. Comm.*, 2013, 49, 7391-7393.
54.   S. R. Shin, C. Zihlmann, M. Akbari, P. Assawes, L. Cheung, K. Zhang, V. Manoharan, Y. S. Zhang, M. Yüksekkaya and K. t. Wan, *Small*, 2016, 12, 3677-3689.
55.   A. Lagazzo, S. Lenzi, R. Botter, P. Cirillo, F. Demicheli, D.T. Beruto, *Particuology*, 2010, 8, 245–250
56.   B. Pukánszky, and G. Vörös, *Polym. Composites*, 1996, *17*, 384-392.
57.   Y. Luo, H. Shen, Y. Fang, Y. Cao, J. Huang, M. Zhang, J. Dai, X. Shi and Z. Zhang, *ACS Appl. Mater. interfaces*, 2015, 7, 6331-6339.
58.   R. Murugan and S. Ramakrishna, *Tissue Eng.*, 2006, 12, 435-447.
59.   T. J. Webster, L. S. Schadler, R. W. Siegel and R. Bizios, *Tissue Eng.*, 2001, 7, 291-301.
60.   T. Raimondo, S. Puckett and T. J. Webster, *Int. J. Nanomedicine*, 2010, 5, 647-652.
61.   W. C. Lee, C. H. Y. Lim, H. Shi, L. A. Tang, Y. Wang, C. T. Lim and K. P. Loh, *ACS Nano*, 2011, 5, 7334–7341.
62. T. Alava, J. A. Mann, C. C. Théodore, J. J. Benitez, W. R. Dichtel, J. M. Parpia and H. G. Craighead, *Anal. Chem.*, 2013, 85, 2754–2759.
63.   J. S. Park, N. I. Goo and D. E. Kim, *Langmuir*, 2014, 30,12587–12595.
64.   E. Alsberg, H. J. Kong, Y. Hirano, M. K. Smith, A. Albeiruti and D.J. Mooney, *J. Dent. Res.*, 2003, 82, 903–908.
65.   T. Gong, J. Xie, J. Liao, T. Zhang, S. Lin, and Y. Lin, *Bone Res.*, 2015, *3*, 15029.
66.   A. Marrella, T. Y. Lee, D. H. Lee, S. Karuthedom, D. Syla, A. Chawla, A. Khademhosseini and H. L. Jang, *Mater. Today*, 2017.
67.   R. Jia, X. Zhang and Y. Chen, *Carbon Lett., 2017,* 22, 42-47.
68.   T. J. Webster, L. S. Schadler, R. W. Siegel and R. Bizios, *Tissue Eng.*, 2001, 7, 291-301.
69.   T. Raimondo, S. Puckett and T. J. Webster, *Int. J. Nanomedicine*, 2010, 5, 647-652.
70   L. Zou, X. Zou X, L. Chen, H. Li, T. Mygind, M. Kassem and C. Bünger, *J. Orthop. Res.*, 2008, 26, 56-64.
71.   B. Ganss, R. H. Kim and J. Sodek, *Crit. Rev. Oral. Biol. Med.*, 1999,10, 79-98.
72.   C. E. Tye, K. R. Rattray, K. J. Warner, J. A. Gordon, J. Sodek, G. K. Hunter and K. A. Goldberg, *J. Biol. Chem.,* 2003, 278, 7949-7955.
73.   V. Subraman, M. Thiyagarajan, N. Malathi and S. T. Rajan, *J. Clin. Diagn. Res.*, 2015, 9, ZE10-13